JOURNAL OF SPACECRAFT AND ROCKETS
Vol. 34, No. 1, January–February 1997

Symmetric Motion Control for Adaptive Structure Based Construction of Large Space Structures

Saburo Matunaga*
Tokyo Institute of Technology, Tokyo 152, Japan
and
Junjiro Onoda†
Institute for Space and Astronautical Science, Kanagawa 229, Japan

The configuration of adaptive structures and the deformation docking used for constructing large space structures is examined. The symmetric adaptive structure, which has symmetric distribution of mass and inertia, is proposed for the deformation docking. In addition, a symmetric motion control is presented. The concept, formulation, and advantages of the symmetric motion control are described. It is shown that there is a reduction of computer requirements, as well as the possibility of obtaining closed-form solutions of workspace, a distribution of singularity points, and a measure of the deformation docking possibility. Numerical and experimental simulations using a four-link structural model are conducted to validate the concepts presented.

Nomenclature

c_i = constant; see Eq. (8)
D = measure of the deformation docking; see Eq. (42)
g = gravitational acceleration, m/s^2
I_i = inertia of moment of the ith link, kg m^2
$J_{p,\,\mathrm{sym}}$ = Jacobian matrix for symmetric motion control; see Eq. (14)
J^T = transpose of matrix J
$J_{v,\,\mathrm{sym}}$, $J_{\omega,\,\mathrm{sym}}$ = components of the Jacobian matrix $J_{p,\,\mathrm{sym}}$; see Eqs. (15) and (17)
J_X, J_Y = components of the Jacobian matrix $J_{v,\,\mathrm{sym}}$; see Eq. (16)
J_{Xi}, J_{Yi} = components of the Jacobian matrix J_X, J_Y in the reference frame; see Eq. (11)
$J^\dagger$ = pseudoinverse of matrix J as $J^T(JJ^T)^{-1}$
ℓ = total length of the link structure, m
ℓ_i = length of the ith link, m
ℓ^* = offset link length, m; see Eq. (3)
M = total mass of the link structure, kg
M_i = mass related dimensionless quantity; see Eq. (4)
m_i = mass of the ith link, kg
n_ℓ = number of links in the link structure, $2N$ or $2N+1$
$\boldsymbol{P}_E$ = position (and attitude) vector of the end effector specified in the inertial frame; see Eq. (9)
$\boldsymbol{P}_i$ = position vector of the ith joint ($0 \le i \le n_\ell$) of the link structure
$\boldsymbol{P}_T$ = position vector of the docking target point
$\boldsymbol{P}_0$ = point on the end effector of the link structure, (X_0, Y_0)
$\boldsymbol{q}$ = joint displacements of the link structure; see Eq. (10)
$\dot{\boldsymbol{q}}_c$ = joint rate command; see Eq. (43)
$\boldsymbol{r}_i$ = position vector of the center of mass of the ith link
s_i = length ratio specifying the position of the center of mass of the ith link
$\boldsymbol{u} \cdot \boldsymbol{v}$ = inner product between the vectors $\boldsymbol{u}$ and $\boldsymbol{v}$
$\boldsymbol{u} \times \boldsymbol{v}$ = outer product between the vectors $\boldsymbol{u}$ and $\boldsymbol{v}$
$\boldsymbol{u} // \boldsymbol{v}$ = vector $\boldsymbol{u}$ is parallel to vector $\boldsymbol{v}$
V_e = expected speed of the end-effector, m/s; see Eq. (43) and Table 1
V^* = functional for the variational workspace problem; see Eq. (22)
$\|\boldsymbol{v}\|$ = Euclidean norm of $\boldsymbol{v}$
X_i, Y_i = components of the ith joint specified in the reference frame
XY = reference frame
x, y = normalized components of the position (X, Y), $2X/\ell$, $2Y/\ell$
$\Delta \boldsymbol{P}$ = $\boldsymbol{P}_T - \boldsymbol{P}_E$; see Eq. (43)
ΔT = sampling time, s
ε_i = normalized length of the ith link, $2\ell_i/\ell$; see Eq. (20)
ε^* = offset normalized link length, $2\ell^*/\ell$; see Eq. (21)
θ_i = relative angle between the ith and the $(i-1)$th link
λ = Lagrange multiplier, or constant in Eqs. (19) and (39)
ρ_i = nondimensionalized mass of the ith link
φ_i = angle of the ith link with X axis

Introduction

SINCE the last decade adaptive structures have attracted enormous research interest. In previous work,[1,2] the authors have proposed an application of the adaptive structure concept to the construction of large space structures. The key element is the notion of deformation docking, which means the docking of adaptive structures by the rigid-body motion and the geometrical change of the whole structure along with a berthing mechanism as a docking device. Both the construction time and the impact of docking can be effectively reduced using adaptive structures.[3]

Many control methods used for robot manipulators[4–8] are applicable to the deformation docking control of adaptive structures; however, we also require some new control strategies particular to deformation docking. The reasons are as follows. 1) In space the reliability of computers is much less than on ground due to the effect of cosmic rays on the electronics. 2) In general, an adaptive structure has a more complex configuration and has many more degrees of freedom than a space robot manipulator. Thus, a space manipulator control formulation applied to these structures results in rather complex equations, which entail high computation cost and large memory usage. 3) Typical robot control methods are developed for

Received Nov. 7, 1994; revision received Aug. 5, 1996; accepted for publication Aug. 15, 1996.

*Research Associate, Department of Mechano-Aerospace Engineering, 2-12-1 O-okayama, Meguro-ku. Member AIAA.
†Professor, Research Division of Space Transportation, 3-1-1 Yoshinodai, Sagamihara. Member AIAA.

dexterous and dedicated tasks, but such control of adaptive structures may be more difficult because of their large and massive structure. 4) Because in the future many large space structures may be periodic and symmetric in shape, it is meaningful to develop a control method around this symmetric nature. 5) Although we can use the conservation laws of linear and angular momentum for control in the case of no external disturbances, for the general case we must treat the nonholonomic constraint due to the angular momentum conservation. This constraint makes the motion more complex. For simple control, it is desirable to avoid the nonholonomic constraint.

The objective is to investigate a deformation docking control method that solves the stated problems. The authors propose that the appropriate adaptive structure for the deformation docking should be a symmetric structure that has a symmetric distribution of mass and inertia. The formulation of the symmetric motion control and the many advantages of this control, including computational reduction, as well as the possibility of obtaining analytical solutions for the workspace, the singularity profile, and a measure of the docking possibility is explained in detail. Numerical simulations and experiments using a four-link structural model are conducted to confirm the validity of symmetric motion control. In these experiments, the drag-free, zero-g characteristics of space are achieved using ball-bearing supports and an in-plane vibrating table.[9]

Symmetric Motion Control

Concept

Symmetric motion refers to motion with respect to the symmetric plane of a symmetric structure. The structure should follow symmetric motion so that the trajectory of the docking device is restricted to a plane determined by the relationship between the positions of the docking device and the target. As such, its behavior will be simpler in the sense that the conservation law of angular momentum does not need to be considered in the formulation, and thus the nonholonomic constraint does not appear. This idea makes it possible to reduce the number of equations of motion, and thus the computational cost of the control is also reduced. In particular, for adaptive structures with very large degrees of freedom, it is desired that the given mission be accomplished with as few degrees of freedom as possible.

Of course, the symmetric condition for the structure can be a very severe restriction. The proposed method, however, exhibits significant robustness as shown later by numerical and experimental simulations.

Formulation

The model used to explain symmetric motion control is a simplified model of the symmetric variable structure, as shown in Fig. 1. The simplified link structure can be regarded as a reference used in the control of the corresponding adaptive structure. The structure is controlled so that its docking device will move in a plane, and only the motion projected onto the plane is considered along with the projected mass and inertia.

We consider a link structure with $n_\ell = 2N$(even), $2N+1$(odd) links, as shown in Fig. 2, equipped with docking devices at both ends. We first assume that there are no external forces and that the initial linear and angular momenta are zero. The coordinate XY, which includes the motion plane, is defined in Fig. 2, where the origin is located at the center of mass of the structure. Y is the symmetric axis of the structure, and the X axis is perpendicular to the Y axis. We call this coordinate frame the reference frame. The symmetric condition is expressed as $\ell_i = \ell_{n_\ell+1-i}$, $\rho_i = \rho_{n_\ell+1-i}$ for each ith link ($1 \le i \le N$), where

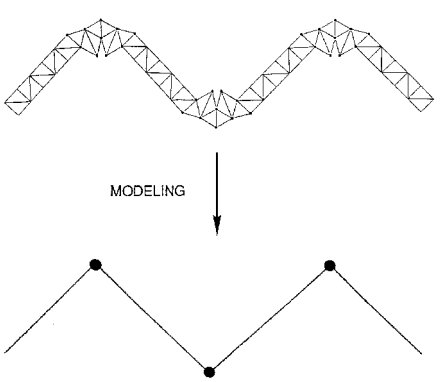

Fig. 1 Reduced link structural model.

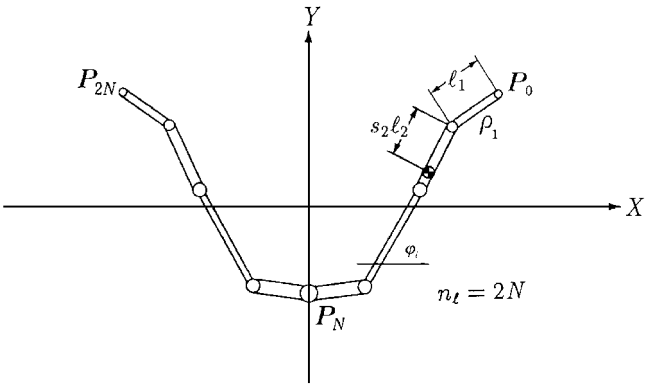

Fig. 2 Analytical model of the link structure.

$$\rho_i = \frac{2m_i}{M}, \qquad \sum_{i=1}^{n_\ell} \rho_i = 2$$

If the center of mass of the ith link $\boldsymbol{r}_i$ is located on the centerline of the link, we can set $\boldsymbol{r}_i = (1 - s_i)\boldsymbol{P}_{i-1} + s_i\boldsymbol{P}_i$, where $0 \le s_i \le 1$.

Since the center of mass of the whole system is located at the origin, the following equation must hold:

$$\sum_{i=1}^{n_\ell} \rho_i \boldsymbol{r}_i = 0 \tag{1}$$

The X component of the equation is identically true because of the symmetric condition. We can derive the following equations from Eq. (1):

$$X_0 = \sum_{i=1}^{N} \ell_i \cos\varphi_i + \ell^*, \qquad Y_0 = \sum_{i=1}^{N} M_i \ell_i \sin\varphi_i \tag{2}$$

$$\ell^* = \begin{cases} 0 & \text{if} \quad n_\ell = 2N \\ \frac{1}{2}\ell_{N+1} & \text{if} \quad n_\ell = 2N+1 \end{cases} \tag{3}$$

$$M_i = 1 - \sum_{j=1}^{i} \rho_j + s_i\rho_i \tag{4}$$

$$\varphi_i = \varphi_N + \sum_{j=i}^{N-1} \theta_j \qquad (1 \le i \le N-1) \tag{5}$$

$$\varphi_N = \begin{cases} \frac{1}{2}\theta_N & \text{if} \quad n_\ell = 2N \\ \theta_N & \text{if} \quad n_\ell = 2N+1 \end{cases} \tag{6}$$

Differentiating with respect to time yields

$$\dot{\varphi}_i = \sum_{j=i}^{N-1} c_j \dot{\theta}_j \qquad (1 \le i \le N) \tag{7}$$

$$c_j = 1 \qquad (1 \le j \le N-1) \tag{8}$$

$$c_N = \begin{cases} \frac{1}{2} & \text{if} \quad n_\ell = 2N \\ 1 & \text{if} \quad n_\ell = 2N+1 \end{cases} \tag{9}$$

Differentiating Eq. (2) gives the following:

$$\dot{X}_0 = \sum_{i=1}^{N} J_{Xi}\dot{\theta}_i, \qquad \dot{Y}_0 = \sum_{i=1}^{N} J_{Yi}\dot{\theta}_i \tag{10}$$

where

$$J_{Xi} = -c_i \sum_{j=1}^{i} \ell_j \sin\varphi_j, \qquad J_{Yi} = c_i \sum_{j=1}^{i} M_j \ell_j \cos\varphi_j \quad (11)$$

Hence, a linear relationship between the rates of the controlled structure's joint variables $\dot{\boldsymbol{q}}$, and the end-effector linear and angular inertial velocities $\dot{\boldsymbol{P}}_E$ can be written as follows.

1) Direct kinematics:

$$\dot{\boldsymbol{P}}_E = J_{p,\,\mathrm{sym}}\,\dot{\boldsymbol{q}} \quad (12)$$

2) Inverse kinematics:

$$\dot{\boldsymbol{q}} = J^{\dagger}_{p,\,\mathrm{sym}}\,\dot{\boldsymbol{P}}_E \quad (13)$$

where

$$\boldsymbol{q} = (\theta_1, \theta_2, \ldots, \theta_N)^T, \qquad \boldsymbol{P}_E = (X_0, Y_0, \varphi_1)^T$$

$$J_{p,\mathrm{sym}} = \begin{bmatrix} J_{v,\mathrm{sym}} \\ J_{\omega,\mathrm{sym}} \end{bmatrix} \quad (14)$$

$$J_{v,\mathrm{sym}} = \begin{bmatrix} J_X \\ J_Y \end{bmatrix} \quad (15)$$

$$J_X = [J_{X1}, J_{X2}, \ldots, J_{XN}], \qquad J_Y = [J_{Y1}, J_{Y2}, \ldots, J_{YN}] \quad (16)$$

$$J_{\omega,\,\mathrm{sym}} = [c_1, c_2, \ldots, c_N] \quad (17)$$

The symmetric motion control uses the Jacobian matrix $J_{p,\,\mathrm{sym}}$ of Eq. (14) or $J_{v,\,\mathrm{sym}}$ of Eq. (15) for a rough control, which may be more appropriate for the deformation docking. The resolved motion-rate control[4–6] or the resolved acceleration control[7] is also applicable. It is clear from Eq. (14) that the computational cost of the symmetric motion control is drastically reduced in comparison with that of conventional control methods.[5,6] This reduction occurs because, in the analysis, it is not necessary to consider the conservation of angular momentum. Yet even considering the initial linear and angular momentum, a simpler control is obtained, and the system is holonomic instead of nonholonomic, as is the case for conventional control methods.[3]

Characteristics of the Symmetric Motion Control

Symmetric Workspace

Generally it is possible to obtain the workspace of a space manipulator only numerically, not analytically. For the symmetric link structure under symmetric motion control, however, we can derive a closed-form solution of the workspace mapped out by the end effector. The boundary of the workspace is obtained by searching the maximum value of Y_0 with the constraint that the value of X_0 is fixed. To clarify the shape of the workspace, the nondimensionalized forms from Eq. (2) are used:

$$x = \sum_{i=1}^{N} \varepsilon_i \cos\varphi_i + \varepsilon^* \quad (18)$$

$$y = \sum_{i=1}^{N} M_i \varepsilon_i \sin\varphi_i \quad (19)$$

where

$$\sum_{i=1}^{n_\ell} \varepsilon_i = 2 \quad (20)$$

$$\varepsilon^* = \begin{cases} 0 & \text{if} \quad n_\ell = 2N \\ \frac{1}{2}\varepsilon_{N+1} & \text{if} \quad n_\ell = 2N+1 \end{cases} \quad (21)$$

Hence, the workspace problem finally becomes the following variational one: maximize the functional $V^* = V^*(\varphi_i, \lambda)$, where

$$V^* = \sum_{i=1}^{N} M_i \varepsilon_i \sin\varphi_i + \lambda \left(\varepsilon^* + \sum_{i=1}^{N} \varepsilon_i \cos\varphi_i - x|_{\mathrm{fix}} \right) \quad (22)$$

Necessary conditions are Eq. (18), as well as the following:

$$M_i \cos\varphi_i - \lambda \sin\varphi_i = 0 \qquad (1 \le i \le N) \quad (23)$$

where $-\pi \le \varphi_i \le \pi$ without loss of generality. Substituting Eq. (23) into Eqs. (18) and (19) produces the solution

$$x = \sum_{i=1}^{N} \frac{\lambda}{\sqrt{M_i^2 + \lambda^2}} \varepsilon_i + \varepsilon^* \quad (24)$$

$$y = \pm \sum_{i=1}^{N} \frac{M_i^2}{\sqrt{M_i^2 + \lambda^2}} \varepsilon_i \quad (25)$$

where $\lambda \ge 0$. The trajectory of the point (x, y) is the boundary of the workspace in the symmetric motion control. As such this workspace is called a symmetric workspace. Note that considering the symmetry of the structure, the boundary of the overall workspace can be regarded as the combined trajectory of the points (x, y) and $(-x, y)$.

Three characteristic solutions are presented. The first is homogeneity:

$$\rho_i = \varepsilon_i = \begin{cases} 1/N & (1 \le i \le N) \quad \text{if} \quad n_\ell = 2N \\ 2/(2N+1) & (1 \le i \le N+1) \quad \text{if} \quad n_\ell = 2N+1 \end{cases}$$

for two cases. The case where operation only hinge(s) at midpoint (one degree of freedom). Here, if $n_\ell = 2N$, then reducing to $N = 1$ into Eq. (25) yields

$$x^2 + 4y^2 = 1 \quad (26)$$

This equation is an ellipse with a major to minor axis ratio of 2:1 as shown in Fig. 3a. Or if $n_\ell = 2N + 1$, then for $x \ge 0$,

$$\left\{ \left(x - \frac{1}{2N+1} \right) \Big/ \frac{2N}{2N+1} \right\}^2 + \left\{ y \Big/ \frac{2N(N+1)}{(2N+1)^2} \right\}^2 = 1 \quad (27)$$

For the case of infinite degrees of freedom: $n \to \infty$, $N \to \infty$, after taking the limit, we have

$$x = \lambda \sinh^{-1}(1/\lambda), \qquad y = (\lambda/2)[\cosh(x/\lambda) - x] \quad (28)$$

Note that the equations can be derived directly from the model of a string.[1]

The second solution is for concentrated mass at the midpoint:

$$\rho_i = \begin{cases} \dfrac{1-\rho_N}{N-1} & (0 \le \rho_N \le 1,\ 1 \le i \le N-1) \quad \text{if} \quad n_\ell = 2N \\ \dfrac{1-\rho_{N+1}/2}{N} & (0 \le \rho_{N+1} \le 2,\ 1 \le i \le N) \quad \text{if} \quad n_\ell = 2N+1 \end{cases}$$

$$\varepsilon_i = \begin{cases} 1/N & (1 \le i \le N) \quad \text{if} \quad n_\ell = 2N \\ 2/(2N+1) & (1 \le i \le N+1) \quad \text{if} \quad n_\ell = 2N+1 \end{cases}$$

As the center of mass increases, the symmetric workspace approaches a circle as shown in Fig. 3b:

$$x^2 + y^2 = 1 \quad (29)$$

where

$$\rho_i \to 0 \begin{cases} (1 \le i \le N-1), & \rho_N \to 1 \quad \text{if} \quad n_\ell = 2N \\ (1 \le i \le N), & \rho_{N+1} \to 2 \quad \text{if} \quad n_\ell = 2N+1 \end{cases}$$

$$\varepsilon_i \to 0 \quad (1 \le i \le N \ \text{ or } \ N+1)$$

and

$$N \to \infty$$

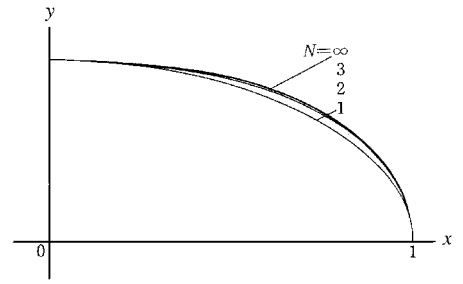

a) Uniform mass distribution

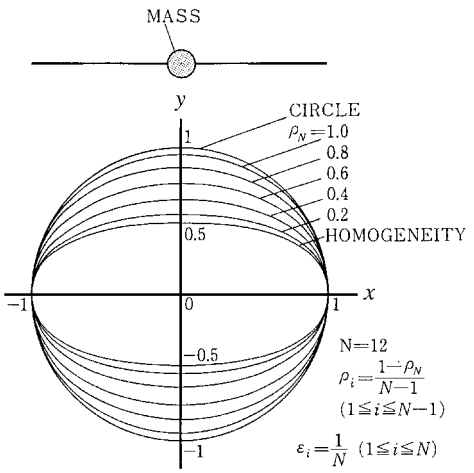

b) Concentrated mass at the center

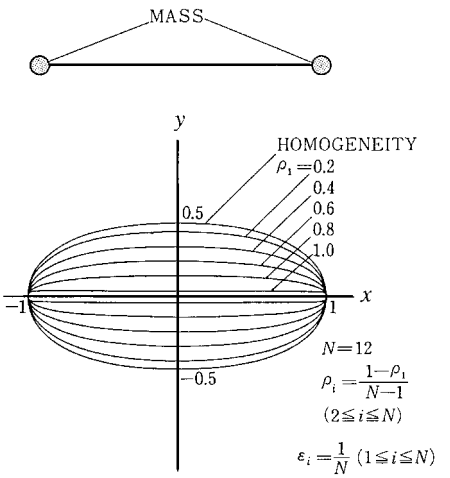

c) Concentrated mass at the both ends

Fig. 3 Symmetric workspaces.

The third solution is for concentrated masses at both ends:

$$\rho_i = \begin{cases} \dfrac{1-\rho_1}{N-1} & (0 \le \rho_1 \le 1,\ 2 \le i \le N) \quad \text{if} \quad n_\ell = 2N \\ \dfrac{1-\rho_1}{N-1/2} & (0 \le \rho_1 \le 2,\ 2 \le i \le N+1) \quad \text{if} \quad n_\ell = 2N+1 \end{cases}$$

$$\varepsilon_i = \begin{cases} 1/N & (1 \le i \le N) \quad \text{if} \quad n_\ell = 2N \\ 2/(2N+1) & (1 \le i \le N+1) \quad \text{if} \quad n_\ell = 2N+1 \end{cases}$$

Figure 3c shows that as the end masses increase, the workspace gradually becomes slender and finally approaches the following equation of a line:

$$y = 0 \qquad (-1 \le x \le 1) \tag{30}$$

where

$$\rho_1 \to 1, \qquad \rho_i \to 0 \qquad (2 \le i \le N \text{ or } N+1)$$

$$\varepsilon_i \to 0 \qquad (1 \le i \le N \text{ or } N+1)$$

and

$$N \to \infty$$

It is clear from Fig. 3 that in space the form of the workspace is strongly dependent on the distribution of mass. This distribution is different from that on the ground. It is also noteworthy that since the symmetric workspace can be calculated with knowledge of only the position and attitude of the reference frame, or the symmetric plane, the workspace can be easily determined even in the case of existence of momentum and external forces.

Figure 3a shows that the symmetric workspace rapidly converges to that of the infinite degree-of-freedomstructure, and the difference in the area is very small. Hence, in general the ellipse with $N = 1$ is a very good area approximating the symmetric workspace. This ellipse can be obtained by letting $\varphi_i = \text{const}$ for all $i\,(1 \le i \le n)$ in Eq. (25) such that

$$(x \mp \varepsilon^*)^2 + \frac{y^2}{\left(\sum_{i=1}^{N} M_i \varepsilon_i\right)^2} = 1 \tag{31}$$

where the sign $-$ and $+$ are used to denote $x \ge 0$ and $x < 0$, respectively. In other words, the area of the symmetric workspace obtained from Eq. (25) as

$$4\int_0^\infty \sum_{i,j=1}^{N} \varepsilon_i \varepsilon_j M_i^2 M_j^2 \left(M_i^2 + \lambda^2\right)^{-1/2} \left(M_j^2 + \lambda^2\right)^{-3/2} \mathrm{d}\lambda \tag{32}$$

may be satisfactorily approximated by the area of the correspondent ellipse of Eq. (31) as

$$\pi \sum_{i=1}^{N} M_i \varepsilon_i \tag{33}$$

This hypothesis has not yet been analytically proven except for some special cases such as the homogeneous mass distribution case and the concentrated mass case. However, a considerable number of numerical simulations have been made to support the hypothesis. This result plays an important role in the determination of the docking possibility to be explained later.

Singularity

For reliability, it is important to characterize the controller singularities. We are concerned with the position, and not the attitude, of the end effector, so that we can use the Jacobian matrix $J_{v,\,\mathrm{sym}}$ of Eq. (15). The singular point is found from the characteristic equation

$$\det\left(J_{v,\,\mathrm{sym}} J_{v,\,\mathrm{sym}}^T\right) = 0 \tag{34}$$

The left-hand side of the preceding equation becomes

$$\begin{aligned} \det\left(J_{v,\mathrm{sym}} J_{v,\mathrm{sym}}^T\right) &= \|J_X\|^2 \|J_Y\|^2 - (J_X \times J_Y)^2 \\ &= \|J_X \times J_Y\|^2 \end{aligned} \tag{35}$$

Hence, a singularity occurs when

$$J_X = \mathbf{0}, \qquad J_Y = \mathbf{0} \tag{36a}$$

$$J_X // J_Y \qquad (J_X \ne \mathbf{0},\ J_Y \ne \mathbf{0}) \tag{36b}$$

Since $c_i > 0$, $\ell_i > 0\,(1 \le i \le N)$, letting $-\pi \le \varphi_i \le \pi$ from the condition of the left-hand equation of Eq. (36a) yields

$$\varphi_i = 0, \qquad \pm\pi \qquad (1 \le i \le N) \tag{37}$$

Similarly, since $M_i > 0\,(1 \le i \le N)$, letting $-\pi \le \varphi_i \le \pi$ from the right-hand equation of Eq. (36a) produces

$$\varphi_i = \pm\pi/2 \qquad (1 \le i \le N) \tag{38}$$

The second condition of Eq. (36b) leads to the following equation:

$$M_i \cos\varphi_i - \lambda \sin\varphi_i = 0 \tag{39}$$

for all $i\,(1 \le i \le N)$.

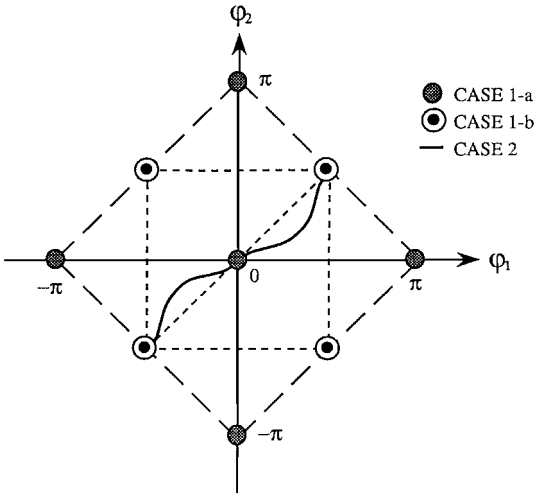

Fig. 4 Singularities in joint space.

The singular points of Eqs. (37) and (38) are related to the link mechanism and are identical to that of the fixed-base condition. These points can be easily avoided, however, because they are located discretely at the joint space, as shown in Fig. 4 for the case of $N = 2$ and $-\pi \leq \varphi_2 + \varphi_1,\ \varphi_2 - \varphi_1 \leq \pi$. On the other hand, Eq. (39) is identical to Eq. (23). Namely, both ends of the structure are on the boundary of the symmetric workspace. The singularity exists continuously in the joint space, as shown in Fig. 4. Thus, we will never cross the singularity curve if we apply a control using the Jacobian $J_{v,\mathrm{sym}}$ of Eq. (15). Note that this is a predictable result.

Therefore, we can conclude that as far as the symmetric motion control method is concerned, we do not encounter the singular point in a practical sense. This result has remarkable merit because it is difficult to obtain similar analytical results for the conventional control methods.

Measure of the Deformation Docking Possibility

Before attempting to dock with a target, it is important to determine whether the deformation docking is possible. We can apply the symmetric workspace from the preceding section to the determination of docking possibility. As long as the target is in the workspace, the docking is certainly possible. We have the closed-form solution of the symmetric workspace, as shown in Eq. (25), which includes two transcendental equations with the parameter λ. The determination of whether the target is included in the area is not so easy. Thus, it is appropriate that we use the approximate workspace, namely, the ellipse, of Eq. (31) in the dimensional form, i.e.,

$$(X \mp \ell^*)^2 + \frac{Y^2}{\left(\sum_{i=1}^{N} M_i \ell_i\right)^2} = \frac{\ell^2}{4} \tag{40}$$

Now it is a very simple matter to determine whether the target is included in the area. Given (X_t, Y_t) as the position of the target expressed in the reference frame, the following scalar D can be defined as a measure of the deformation docking:

$$D(X_t, Y_t) = \frac{\ell^2}{4} - \left(X_t \mp \ell^*\right)^2 - \frac{Y_t^2}{\left(\sum_{i=1}^{N} M_i \ell_i\right)^2} \tag{41}$$

The docking possibility is then determined as follows:

$$D \begin{cases} >0\text{: docking possible} \\ \leq 0\text{: docking impossible} \end{cases} \tag{42}$$

The measure D gives a good, safe evaluation of the docking possibility because the ellipse of Eq. (40) is a good, conservative approximation of the area of the symmetric workspace.

Simulations of the Symmetric Motion Control

Numerical Simulations

Numerical simulations are performed using a four-link structural model, as shown in Fig. 5. Model specifications are given in Table 1. A small shift from the symmetric distribution of mass and inertia is imposed to test the robustness of the symmetric motion control. It is assumed that no external forces exist and that the initial linear and angular momentum are identically zero. Although the link structure has three degrees of freedom, the symmetric motion control uses two degrees of freedom of the structure, considering the position of the end effector. Thus, the control is expressed as follows, using Eq. (15) with the resolved motion rate control[4]:

$$\dot{\boldsymbol{q}}_c = J_{v,\mathrm{sym}}^{-1}(\boldsymbol{q}) \frac{\Delta \boldsymbol{P}}{\|\Delta \boldsymbol{P}\|} V_e \tag{43}$$

where $\Delta \boldsymbol{P} = \boldsymbol{P}_T - \boldsymbol{P}_E$ is measured at every sampling time, as in vision feedback control. The ellipse of Eq. (40) is used as a measure of docking possibility in the simulations.

To estimate the performance of the symmetric motion control, we compare it to both the conventional control[6] and the semisymmetric motion control in the case that the structure is forced to follow symmetric motion by the conventional control. In both control methods, the control performance is generally expected to be better than that of the proposed symmetric control because all of the kinematic information of the structure is used, but the computation cost is higher. Figure 6 shows results of the docking simulations. In Fig. 6a, 1) initial shows the initial positions of the structure ($\theta_1 = \theta_3 = -120,\ \theta_2 = 120$ deg) and the target, 2) conventional shows the results using the conventional control, 3) semisymmetric shows the results using the semisymmetric motion control, and 4) symmetric shows the results using the symmetric motion control. Figure 6b shows a plot of the measured speed of the end effector. For the symmetric motion control, there is a difference between the measured speed and the expected value V_e, due to the shift of mass and inertia distribution. This difference is small and, in addition, the behavior is as smooth as that for the conventional control. Similar results are seen for many other simulations when the target is located near the end of the major axis of the ellipse. It was also confirmed that as long as the target is located in the ellipse, the docking is possible. Thus, the ellipse can be used as a measure of docking possibility. Note that even in the case that the initial posture is asymmetric, regardless of the initial condition, the symmetric motion control can be successfully applied with the help of vision feedback and that the ellipse, however, can not be used as the measure in general.

Table 1 Specification of parameters

		Link 1	Link 2	Link 3	Link 4
Length	ℓ_i, m	0.300	0.300	0.300	0.300
	s_i	0.410	0.500	0.500	0.427
Mass	m_i, kg	1.235	1.011	1.168	1.182
Inertia	I_i, kg m^2	0.0272	0.0232	0.0255	0.0263
Sampling time		ΔT, s	0.4		
Speed of end effector		V_e, m/s	0.03		

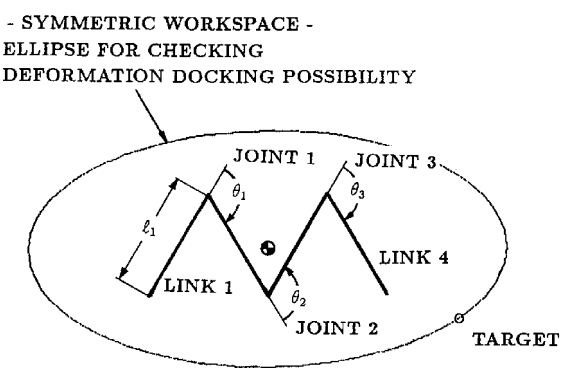

Fig. 5 Description of the link structure.

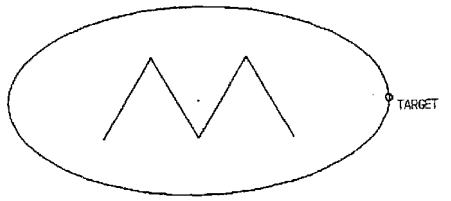

1) Initial

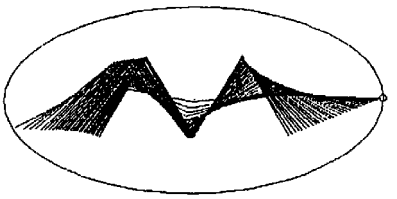

2) Conventional

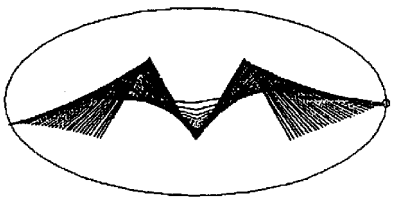

3) Semisymmetric

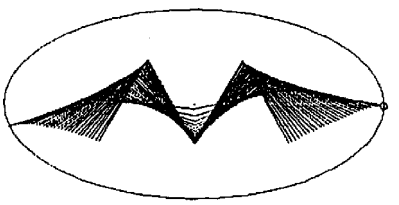

4) Symmetric

a) Trace of sensed motion

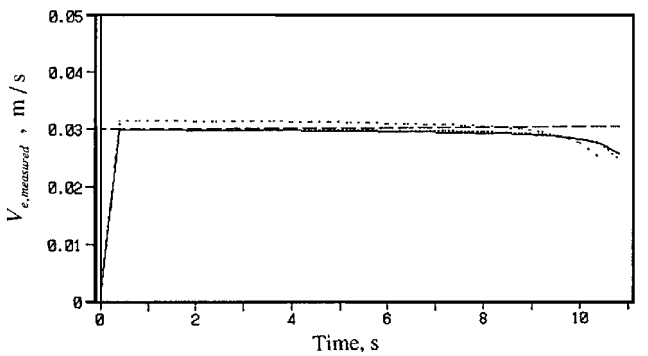

b) Velocity of the end effector

Fig. 6 Numerical simulations: ——, conventional; · · · · ·, semisymmetric; and ·· · ··, symmetric.

Experimental Simulations

Experimental simulations of the deformation docking were conducted to verify the preceding results. A gravity compensation system using the sliding compensation method with an in-plane vibrating table is applied.[9] The sliding compensation uses the fact that the effective coulomb friction is diminished using a vibrating table, namely, by the dither effect.

Figure 7 shows an outline of the link structural model used in this experiment. Specifications are the same as for the numerical simulations and are given in Table 1. The link structure with five ball-bearing supports has three degrees of freedom in rotation. Figure 8 shows a block diagram of the experimental setup. The testbed is composed of an in-plane vibrating table (1200 × 1200 mm), a position sensor consisting of infrared light emitting diodes and a camera, and a personal computer to drive the A/D and D/A converters. The

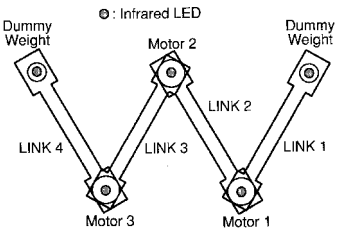

Fig. 7 Experimental model of the link structure.

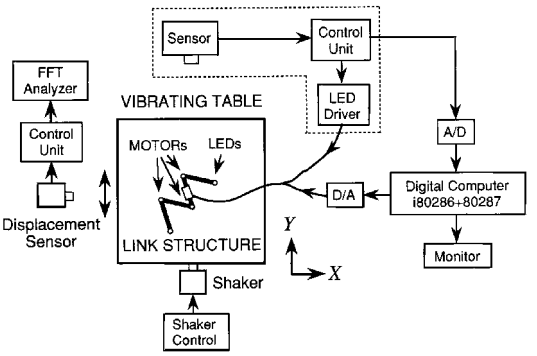

Fig. 8 Schematic view of the experimental setup, position sensor system.

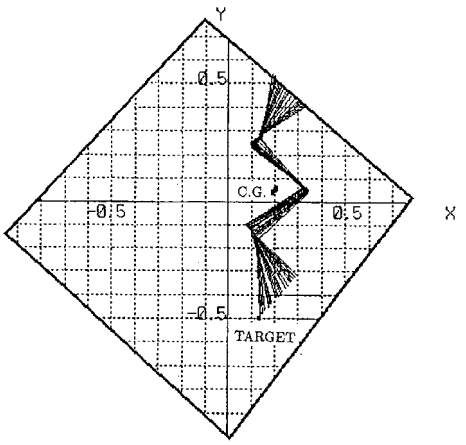

a) Trace of sensed motion

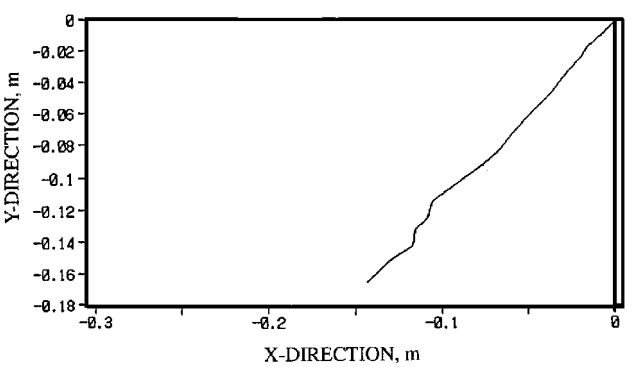

b) Velocity of the end effector

Fig. 9 Experimental results.

frequency and amplitude of the vibrating table are measured by an optical displacement gauge and a fast Fourier transform analyzer. The errors of sensed positions due to the orientation of the camera and other parameters are corrected by an iterative least squares method. The positions are sensed by a camera suspended at a height of 3 m, and the maximum position error is 9 mm (Ref. 3).

The control law is the same as Eq. (43) in the numerical simulations. The ellipse of Eq. (40) is also used as a measure of the docking possibility. Figure 9 shows the experimental results. Figure 9a

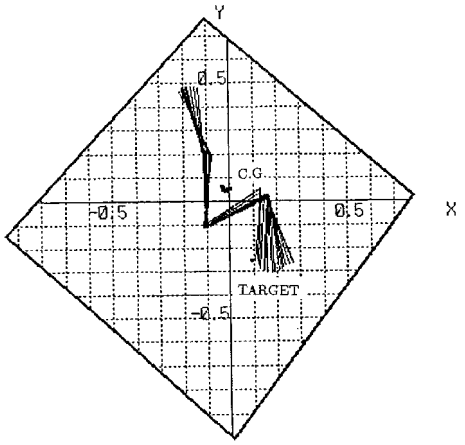

a) Trace of sensed motion

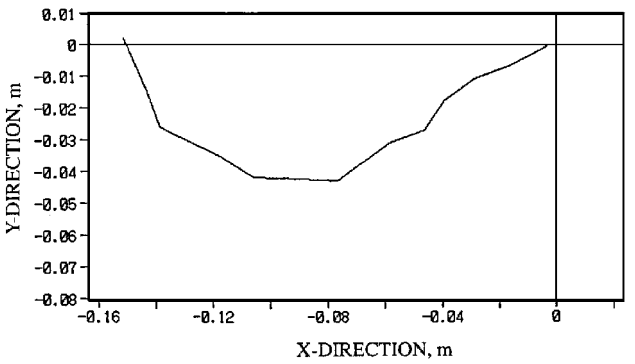

b) Velocity of the end effector

Fig. 10 Experimental results, asymmetric initial posture.

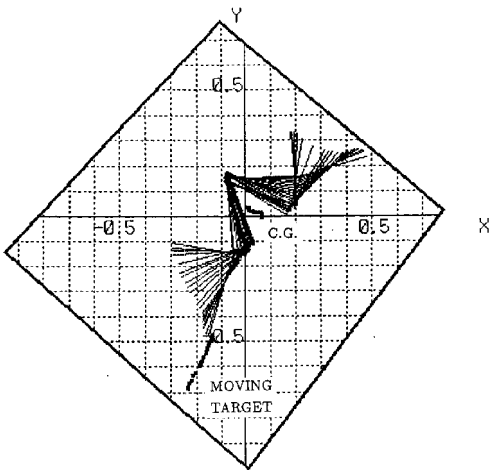

Fig. 11 Experimental results, moving target.

represents the trace of sensed motion of the structure where the curve of black points indicates the trajectory of the center of mass of the whole structure. Figure 9b represents the trajectory of the end effector with respect to the initial position. The trajectory is expected to be a straight line under the control of Eq. (43). Considering the estimation error of the position by the camera ($\pm 2 - \pm 5$ mm on average) and the shift of mass and inertia distribution of the structure, we can conclude that this is a good result. Many experiments show that as long as the target is located in the ellipse, docking is possible. Figures 10 and 11 show that even in the case that the initial posture is asymmetric or that the target is moving (velocity approximately 0.015 m/s), the deformation docking using symmetric motion control is successfully performed with the aid of vision feedback.

Summary and Conclusions

The authors propose that an appropriate adaptive structure for deformation docking should be a symmetric structure that has symmetric distribution of mass and inertia, and that the docking control method should be a symmetric motion control.

The concept, formulation, and advantages of the symmetric motion control are outlined. The behavior of the structure under symmetric motion control becomes simpler in the sense that the conservation law for angular momentum does not need to be considered in the formulation; therefore, the nonholonomic condition does not appear. The method makes it possible to reduce the number of equations of motion, and thus the computational cost of the control is also reduced. The closed-form solutions of workspace of the end effector can be obtained by the variational method, and the singularity profile of the workspace can also be determined analytically. It is shown that under symmetric motion control the system does not fall into the singular point in a practical sense. The authors show that the a given ellipse is a good, conservative approximation of the area of the workspace, and propose a measure of deformation docking possibility using this ellipse.

The validity of symmetric motion control was successfully confirmed by the results of numerical and experimental simulations using a four-link structural model with the aid of vision feedback.

Acknowledgments

The authors thank K. Ichida of the Institute for Space and Astronautical Science for his cooperation with the experiments and Y. Ohkami of the Tokyo Institute of Technology for his valuable comments.

References

[1]Miura, K., and Matunaga, S., "An Attempt to Introduce Intelligence in Structures," *Proceedings of AIAA/ASME/ASCE/AHS/ASC 30th Structures, Structural Dynamics and Materials Conference* (Mobile, AL), AIAA, Washington, DC, 1989, pp. 1145–1153 (AIAA Paper 89-1289).

[2]Matunaga, S., Miura, K., and Natori, M., "A Construction Concept of Large Space Structures Using Intelligent/Adaptive Structures," *Proceedings of AIAA/ASME/ASCE/AHS/ASC 31st Structures, Structural Dynamics and Materials Conference* (Long Beach, CA), AIAA, Washington, DC, 1990, pp. 2298–2305 (AIAA Paper 90-1128).

[3]Matunaga, S., "On Construction Method of Large Space Structures Using Intelligent/Adaptive Structures," Ph.D. Dissertation, Dept. of Aeronautical Engineering, Univ. of Tokyo, Japan, Sept. 1991.

[4]Whitney, D. F., "Resolved Motion Rate Control of Manipulators and Human Prostheses," *IEEE Transactions of Man–Machine System*, Vol. MMS-10, 1969, pp. 47–53.

[5]Umetani, Y., and Yoshida, K., "Continuous Path Control of Space Manipulators Mounted on OMV," *Acta Astronautica*, Vol. 15, No. 12, 1987, pp. 981–986.

[6]Masutani, Y., Miyazaki, F., and Arimoto, S., "Sensory Feedback Control for Space Manipulators," *Proceedings of IEEE International Conference on Robotics and Automation* (Scottsdale, AZ), Inst. of Electrical and Electronics Engineers, Piscataway, NJ, 1989, pp. 1346–1351.

[7]Luh, J., Walker, M., and Paul, R. G., "Resolved Acceleration Control of Mechanical Manipulators," *IEEE Transactions on Automatic Control*, Vol. AC-25, No. 3, 1980, pp. 468–474.

[8]Vafa, Z., and Dubowsky, S., "On the Dynamics of Manipulators in Space Using the Virtual Manipulator Approach," *Proceeding of 1987 IEEE International Conference on Robotics and Automation* (Raleigh, NC), Inst. of Electrical and Electronics Engineers, Piscataway, NJ, 1987, pp. 579–585.

[9]Matunaga, S., and Onoda, J., "A New Gravity Compensation Method by Dither for Low-G Simulation," *Journal of Spacecraft and Rockets*, Vol. 32, No. 2, 1995, pp. 364–369.

F. H. Lutze Jr.
Associate Editor